Energy & Environmental Science

Accepted Manuscript

ROYAL SOCIETY OF CHEMISTRY

www.rsc.org/ees

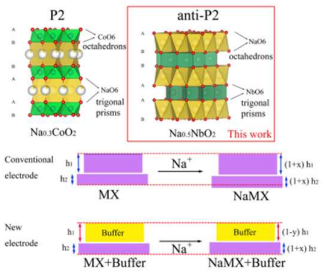

Layer-structured anti-P2 $Na_{0.5}NbO_2$ composed of NbO_6 trigonal prisms and NaO_6 octahedrons shows a negative strain effect: its lattice shrinks upon Na-ion intercalation and expands upon deintercalation.

Layer-structured oxides are the basis subject for their essential roles in various applications (*e.g.* high-energy batteries and superconductors) due to their distinctive physical structures and chemical properties. Most of the layered A_xMO_2 (A = alkali ions, M = transition metals) are composed of MO_6 octahedrons and varied A coordination polyhedron such as octahedrons (O), tetrahedrons (T) or trigonal prisms (P). Herein, we report a new layered oxide anti-P2 Na0.5NbO2 material with two unusual characteristics: 1) NbO_6 trigonal prisms and NaO_6 octahedrons; 2) negative volume or strain effect. That is, its lattice shrinks upon sodium (Na)-ion intercalation and expands upon Na-ion deintercalation. Moreover, $Na_{0.5}NbO_2$ exhibits high structural stability, long cycle life and prominent rate performance for Na-ion batteries. These distinctive features make $Na_{0.5}NbO_2$ promising either as an excellent independent active electrode material or as a "volume buffer" in constructing long-lifespan composite electrode with *positive-strain* materials. Our findings will arouse great attention on anti-P2 layered oxides for material science and applications, and develop an effective way of "volume buffer" to achieve high energy density batteries with long life.

Energy & Environmental Science

RSCPublishing

ARTICLE

Anti-P2 structured $Na_{0.5}NbO_2$ and Its Negative Strain Effect

Cite this: DOI: 10.1039/xoxxoooooox

Xuefeng Wang[a]‡, Yurui Gao[a]‡, Xi Shen[b], Yejing Li[a], Qingyu Kong[c], Sungsik Lee[c], Zhaoxiang Wang[a]*, Richeng Yu[b], Yong-Sheng Hu[a] and Liquan Chen[a]

Received ooth January 2012,
Accepted ooth January 2012

DOI: 10.1039/xoxxoooooox

www.rsc.org/

Layer-structured oxides are the basis subject for their essential roles in various applications (*e.g.* high-energy batteries and superconductors) due to their distinctive physical structures and chemical properties. Most of the layered A_xMO_2 (A=alkali ions, M= transition metals) are composed of MO_6 octahedrons and varied A coordination polyhedron such as octahedrons (O), tetrahedrons (T) or trigonal prisms (P). Herein, we report a new layered oxide material, anti-P2 $Na_{0.5}NbO_2$, which is composed of NbO_6 trigonal prisms and NaO_6 octahedrons. Its lattice shrinks as sodium (Na) ions are intercalated in it and expands when the ions are deintercalated (a negative volume or strain effect). Analysis by X-ray absorption spectroscopy and density functional theory (DFT) calculations indicates that the negative volume effect is mainly a result of the enhanced interlayer (Na-O) interaction and the weakened Nb-Nb and Nb-O bonding in the O-Nb-O slab upon Na intercalation. Moreover, $Na_{0.5}NbO_2$ exhibits high structural stability, long cycle life and prominent rate performance for Na-ion batteries. These distinctive features make $Na_{0.5}NbO_2$ an ideal "volume buffer" to compensate for the *positive-strain* electrode materials. These findings will arouse great attention on anti-P2 layered oxides for material science and applications, and enrich the understanding of a novel *negative-strain* material for energy storage either as an excellent independent active electrode material or as a volume buffer in constructing long-life composite electrode with *positive-strain* materials.

Introduction

Layer-structured materials have been extensively exploited and have shown great potential in various applications due to their unique crystal structures and physical/chemical properties. Specifically, layered oxides with formula A_xMO_2 (A=alkali ions, M= transition metals) are of great interest as the electrode materials for rechargeable batteries. [1-6] Most A_xMO_2 are composed of $(MO_2)_n$ sheets with edge-sharing MO_6 octahedrons, between which are the alkali atoms located with octahedral (O), tetrahedral (T) or prismatic (P) environments. [7-11] Based on the stacking mode of the $(MO_2)_n$ sheets, these layered oxides can be further categorized into O3, T1, P2, and P3 types, *etc.*, [12-15] as Delmas *et al.* [16] suggested. However, as will be seen in this article, layered $Na_{0.5}NbO_2$ exhibit a different structure from these layered AMO_2 materials. The NbO_6 clusters in $Na_{0.5}NbO_2$ are edge-sharing trigonal prisms rather than octahedrons, similar to the structure of 2H-type transition metal chalcogenides. We donate such a structure as anti-P2 herein though *anti-* usually means interchange between the anions and the cations rather than between the cations in solid state chemistry. Such layer-structured materials have been rarely exploited; their distinctive properties (electrical, magnetic, optical properties and intercalation chemistry) remain unclear or unknown. [17-20] Similar to or maybe beyond the well-known layer-structured Na_xCoO_2, [7, 21] $Na_{0.5}NbO_2$ are expected to find important applications in various fields such as superconductor and high-energy batteries. [22-27]

Energy storage is essential to the efficient use of renewable energies. Nowadays, the most challenging issues on the rechargeable batteries (*e.g.* lithium (Li)- and sodium (Na)-batteries, *etc.*) are to discover new active materials and develop new techniques to increase the energy density and cycle life of the existed materials for batteries. [28-31] Layered- (*e.g.* $ACoO_2$) and/or framework- (*e.g.* olivine, NASICON, and Prussian blue derivatives) structured materials are the top active materials due to their stable structure and large interstitials spaces. [32-37] On the basis of their behaviors in volume change upon foreign ion insertion, these materials can be classified into positive- (volume expansion), zero- (negligible volume variation) or negative- (volume contraction) strain types. Most of the known active materials are positive-strain types. Their significant positive volume changes have been proved detrimental and are often involved in the inferior long-term cycling stability and safety of the batteries. 'Zero-strain' materials, such as $Li_4Ti_5O_{12}$ (*vs.* Li) and P2-$Na_{0.66}[Li_{0.22}Ti_{0.78}]O_2$ (*vs.* Na), [38-40] are ideal

electrode materials but very rare. Contrary to the positive-strain materials, negative-strain materials are regarded as 'abnormal' species and their functional mechanisms remain unclear. [9, 13, 23, 41-43] Therefore, it is essential to explore new negative-strain materials, to understand their distinctive properties, and to find applications for them either as an excellent independent active electrode material or as a volume buffer in constructing long-life composite electrode with positive-strain materials.

In this work, we report such a layer-structured material, anti-P2 $Na_{0.5}NbO_2$, with unique NbO_6 trigonal prisms and NaO_6 octahedrons, and rare negative-strain character. It shows high structural stability, long cycling life, and prominent rate performance. Its negative volume effect upon Na ion intercalation and deintercalation is comprehensively explored by *in situ* X-ray diffraction (XRD), X-ray absorption spectroscopy (XAS) and density functional theory (DFT) calculations. These distinctive features make $Na_{0.5}NbO_2$ an ideal "volume buffer" for positive-strain electrode materials. As an example of the application of this *buffer* concept, simple composites with positive-strain materials, such as MoS_2, TiO_2 and $Na_2Ti_3O_7$, are prepared and show better cycling stability than the positive-strain materials alone. Our findings enrich the understanding of anti-P2 $Na_{0.5}NbO_2$ with unique MO_6 trigonal prisms and stable layered structure, and develop an effective way of "volume buffer" to achieve high energy density batteries with long life.

Results and discussions

Unique Structure of $Na_{0.5}NbO_2$

Layer-structured $Na_{0.5}NbO_2$ was obtained by solid-state reaction at 800 °C in an evacuated silica tube. The atomic ratio of Na/Nb atoms in the as-prepared material is determined to be 0.5 by inductively coupled plasma-optical emission spectroscopy (ICP), lower than the reported compounds Na_xNbO_2 (x=0.66 and 1).[17, 44] Figure 1a shows the XRD pattern of the as-prepared $Na_{0.5}NbO_2$. Most of its diffraction peaks can be indexed to a hexagonal phase of space group P63/mmc. On the basis of the isostructure to anti-P2 $Na_{0.66}NbO_2$, [17] the lattice parameters of $Na_{0.5}NbO_2$ are refined to be *a* (= b) =2.94 Å and *c*=12.09 Å by TOPAS program fitting (the refined atomic positions are shown in Table S1); the *c* value of $Na_{0.5}NbO_2$ is larger than that of $Na_{0.66}NbO_2$ (*c*=11.69 Å). The additional weak diffractions are assigned to the orthorhombic $NaNbO_3$, a by-product of the highly O_2-sensitive $Na_{0.5}NbO_2$ at high temperatures.

The atomic structure of $Na_{0.5}NbO_2$ was recognized by the aberration-corrected scanning transmission electron microscopy (STEM; it is difficult to obtain higher-quality STEM images along the [100] zone axis because it is hard to ultrasonically exfoliate the compressed large particle even in a polar organic solvent. The particles become amorphous when focused ions beam (FIB) technique is used to make them thinner). As is expected, hexagonally arranged atoms are observed in the high-angle annular dark field (HAADF) (Figure 1b) and annular bright field (ABF) (Figure 1c) images along the [001] zone axis. Furthermore, the Na ions occupy the hollow center of the hexagonal lattice of NbO_2 with octahedral environments.

On the basis of the XRD and STEM results, the schematical structure of $Na_{0.5}NbO_2$ is illustrated in Figure 1d. It is composed of $(NbO_2)_n$ slabs of edge-sharing NbO_6 trigonal prisms, between which are the Na atoms inserted with octahedral environments. This is different from the other layer-structured AMO_2 oxides composed of MO_6 octahedrons and can be regarded as an anti-P2 type with interchanged atomic environments between the alkali ions (A) and transition metals (M) (a typical schematic structure is shown in Figure S1). Although it is difficult to distinguish the P2 and anti-P2 type phases from XRD patterns when they share the same lattice parameters (Figure S2), the latter is proved to be more stable for $Na_{0.5}NbO_2$ by the DFT calculations (Figure 1e). In addition, the lattice parameters of its relaxed structure (Figure 3a) and the refined XRD pattern on the basis of anti-P2 structure are closer to the measured ones. Therefore we believe that the as-prepared $Na_{0.5}NbO_2$ has an anti-P2 structure.

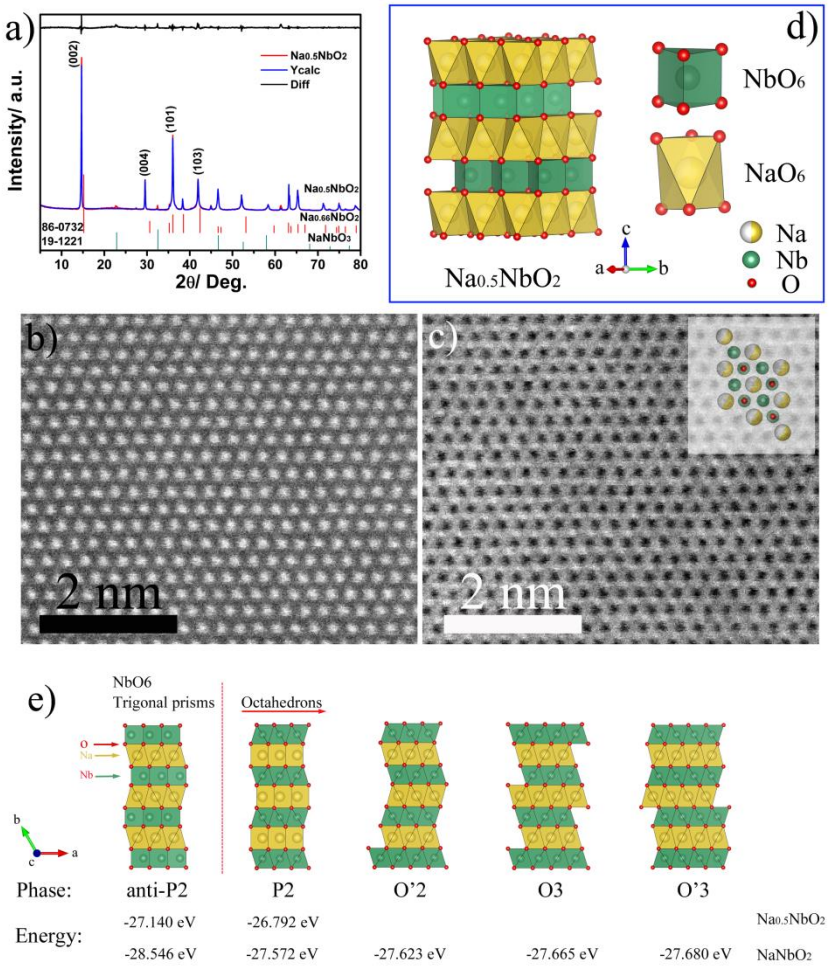

Figure 1. XRD pattern (a), HAADF (b) and ABF (c) images along the [001] zone axis of $Na_{0.5}NbO_2$, its schematic structure (d), and the DFT calculated energy of Na_xNbO_2 (x=0.5 and 1) with trigonal prisms structure and with octahedral structure (f.u., Na_xNbO_2 formula unit (e). The XRD and STEM results demonstrate that the structure of $Na_{0.5}NbO_2$ is composed of $(NbO_2)_n$ slabs of edge-sharing NbO_6 trigonal prisms, between which the Na atoms are inserted with octahedral environments.

Negative volume effect upon Na-ion intercalation

To investigate the intercalation chemistry of $Na_{0.5}NbO_2$, electrochemical intercalation of Na ions was performed in a galvanostatic mode. The intercalation potential profile is shown in Figure 2a (right). A discharge plateau (at about 0.75 V) and two slopes (1.50~0.75 V and 0.75~0.0 V) can be recognized, probably corresponding to the biphasic transition and solid solution reaction, respectively. In order to clarify this intercalation mechanism, *in situ* XRD was performed and the results are shown in Figure 2a (left). The XRD patterns clearly confirm the above deduction. In the solid-solution domain, the prominent (00*l*) (*l*=2 and 4) peaks gradually shift to the higher angles with continuous intercalation of Na ions. In the case of biphasic transition process, the diffraction peaks of $Na_{0.5}NbO_2$ fade, and new peaks for hexagonal $NaNbO_2$ appear and become dominant with further discharging. Intercalation of more Na ions (specific capacity >120 mAh/g or over 0.5 Na per formula of $Na_{0.5}NbO_2$ intercalated) does not lead to any detectable further structural changes, mainly due to the decomposition of the electrolyte and the electrode binder polytetrafluoroethylene (PTFE).

The lattice parameter *a* of hexagonal Na_xNbO_2 is an average of in-plane Nb-Nb distance and its *c* is twice the interlayer spacing. Figure S3 shows that the *c* value of Na_xNbO_2 decreases gradually with continuous intercalation of Na ions. Meanwhile, the *a* value of the discharge product $NaNbO_2$ is refined to be 2.95 Å, slightly larger than that of $Na_{0.5}NbO_2$ (2.94 Å), suggesting that the in-plane Nb-Nb distance is slightly enlarged due to Na-ion intercalation. As a result, the cell volume shrinks due to the largely reduced *c* value during Na intercalation. These seem 'abnormal' and contrary to the behavior (volume expansion) of most other materials upon ion insertion. For example, the volume of $Na_2Ti_3O_7$ [45, 46] and MoS_2 [47] expands by about 6% and 27%, respectively, upon Na insertion. Significantly, the structural change of $Na_{0.5}NbO_2$ is reversible in the subsequent deintercalation (Figure S4a) and reintercalation (Figure S4b) reactions. These behaviors are called a negative volume effect.

To further understand the negative volume effect, X-ray absorption spectroscopic (XAS) data at the Nb K-edge were recorded to detect the valence changes of Nb and local structural changes of $Na_{0.5}NbO_2$ during Na intercalation. Figure 2b shows the X-ray absorption near edge spectroscopic (XANES) results of fresh and fully discharged $Na_{0.5}NbO_2$ at the Nb K-edge. The absorbing edge shifting towards the lower energy indicates that the Nb ions are reduced to some extent. Figure 2c shows the magnitude of Fourier-transformed extended X-ray absorption fine structure (FT-EXAFS) spectra. Compared with fresh $Na_{0.5}NbO_2$, the fully discharged sample has longer Nb-Nb and Nb-O bonds and shorter Nb-Na bonds; the former is consistent with the enlarged *a* value. Therefore, the negative volume effect is a result of the enhanced interlayer (Na-O) interaction and the weakened Nb-Nb and Nb-O bonding in the O-Nb-O slab due to the reduction of the Nb ions upon Na-ion intercalation.

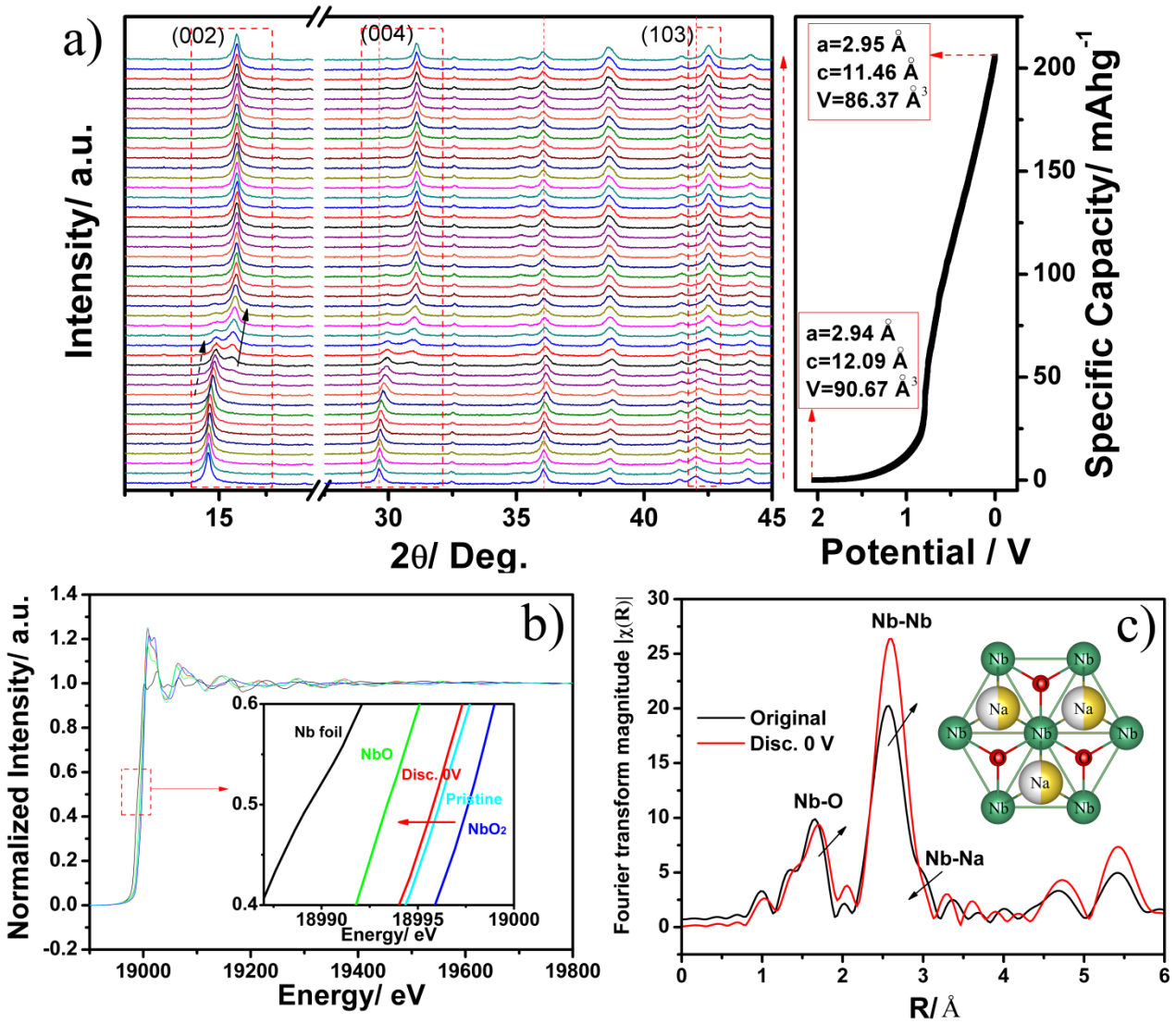

Figure 2. *In situ* XRD patterns of $Na_{0.5}NbO_2$ recorded during electrochemical intercalation of the Na ions (a), the XANES (b) and FT-EXAFS (c) spectra of the fresh and fully discharged (0.0V) $Na_{0.5}NbO_2$. The inset in b is the zoomed edge shift. The FT-EXAFS spectra were not phase-corrected and the shown bond length is shorter than the actual. The results show that the negative volume changes of $Na_{0.5}NbO_2$ originate from the weakened Nb-Nb and Nb-O bonding in the O-Nb-O slab due to reduction of the Nb ions and the enhanced interlayer interaction upon Na intercalation.

Understanding of the negative volume effect by DFT

DFT calculations were conducted to understand the negative volume effect of $Na_{0.5}NbO_2$. Interchanges of O2, O3 or P2, *etc.* are often observed in layer-structured oxides upon ion insertion.[7, 8, 10, 48] However, in this case, the NbO_6 trigonal prisms in $NaNbO_2$ (0.5 Na ions per formula intercalated into $Na_{0.5}NbO_2$)

are energetically more favorable than the NbO_6 octahedrons (total energy about -28.55 *vs.* -27.68 eV per formula unit; Figure 1e). This energy barrier stabilizes the NbO_6 trigonal prisms and prevents the transition from anti-P2 phase to O2, O3 or P2, *etc.* during Na-ion intercalation/deintercalation in $Na_{0.5}NbO_2$, which is crucial for maintaining its native distinctive characters and ensuring the cycling stability.

Figure 3a compares the relaxed structure of $Na_{0.5}NbO_2$ and $NaNbO_2$. Upon intercalation, the lattice parameter *a* (= *b*) of $Na_{0.5}NbO_2$ increases slightly from *ca.* 2.994 to 3.007 Å while its *c* shrinks from 12.003 to 11.705 Å, consistent with the above XRD results (Figure 2a). Besides, the structural symmetry becomes higher when $Na_{0.5}NbO_2$ is transferred to $NaNbO_2$ since the lengths of the Nb-O bonds are the same in the latter (2.185 Å) but range between 2.106 and 2.181 Å in the former. In addition, the NbO_6 prisms accept electrons during intercalation, leading to the reduction of the Nb ions and increase of their ionic radii (Figure S5), and the resultant increase of *a*. Although slight expansion of the NbO_6 trigonal prisms (about 2.494 *vs.* 2.652 Å) occurs along the *c* axis, the obvious shrinkage of the NaO_6 octahedrons (about 3.506 *vs.* 3.201 Å) is responsible for the above *c* reduction.

The density of states (DOS) (Figure 3b) indicates that $Na_{0.5}NbO_2$ is metallic. The states below the Fermi level (energy from -6.7 to -2.3 eV) are mainly a hybridization of the O 2p and Nb 4d orbitals, corresponding to the Nb-O bonding. On the other hand, most of the states near the Fermi level (energy from -0.74 to 1.42 eV) are from electrons in the Nb 4d orbitals, referred to a strong Nb-Nb bonding. [49] The charge distributions (Figure 3d) clearly show that the Nb 4d and O 2p orbitals are isolated in this energy range, while the Nb 4d orbitals are overlapped, forming the strong trigonal Nb-Nb bonds and conduction network for electron transfer.

When the Na ions are intercalated into $Na_{0.5}NbO_2$, the electrons occupy the holes above the Fermi level and fill in the above Nb-Nb network. As a result, more negative charges in the NbO_6 trigonal prisms and more positive charges in the NaO_6 octahedrons pull the adjacent NbO_6 trigonal prisms closer, where the intercalated Na ions act as a bridge to the two NbO_6 blocks. This explains why the lattice parameter *c* shrinks upon Na intercalation. Additionally, a comparison of the charge distribution of the Nb-O bonding states (energy from -6.7 to -2.3 eV) (Figure 3c) between $Na_{0.5}NbO_2$ and $NaNbO_2$ demonstrates that the Nb-O binding strength becomes weaker, in agreement with the increased bond length in $NaNbO_2$. Moreover, the DOS (Figure S6) indicates that $NaNbO_2$ is a semiconductor with a band gap of 1.5 eV.

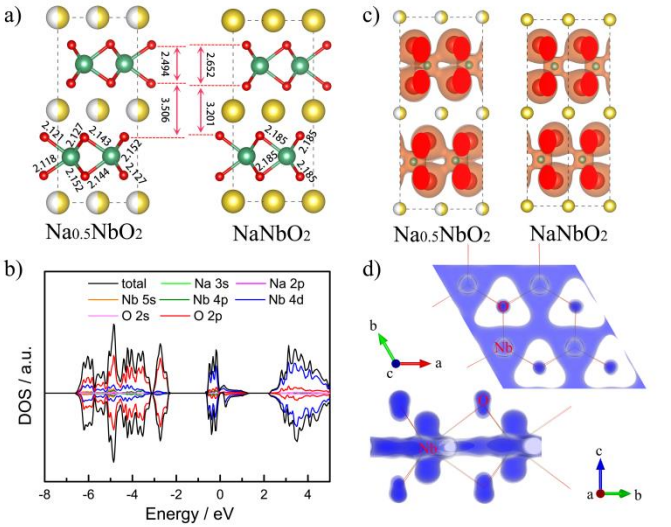

Figure 3. Projection of the calculated structures of $Na_{0.5}NbO_2$ and $NaNbO_2$ along *a* axis (a), partial DOS of atoms in $Na_{0.5}NbO_2$ (b), charge distribution mapping for bonding states with energy from -6.7 to -2.3 eV of $Na_{0.5}NbO_2$ and $NaNbO_2$ (c) and for states near the Fermi level from -0.74 to 1.42 eV of $Na_{0.5}NbO_2$ (d). The Fermi level is set to zero. The DOS indicates that $Na_{0.5}NbO_2$ is metallic. The overlap of Nb 4d orbitals form the strong trigonal Nb-Nb bonding and conduction network for electron transfer, which are responsible for the negative volume effect of $Na_{0.5}NbO_2$.

$Na_{0.5}NbO_2$ as volume buffer in composite electrode

In light of its negative volume effect, $Na_{0.5}NbO_2$ can be used as a volume buffer to improve the cycling performance of the electrode materials with positive volume effects (Figure 4a). Significant and repeated volume expansion and contraction of an electrode material upon ion extraction and insertion will lead to structural fatigue and even particle pulverization, and therefore, capacity decay. The unique negative volume effect of $Na_{0.5}NbO_2$ makes it a potential 'volume buffer' by forming composite with other advanced electrode materials that have a positive volume effects. In order to reach such composite electrode, an ideal volume buffer is supposed to have at least the following characteristics as well as obvious negative volume effect: 1) reversible in structural variation for long-term cycling; 2) compatible with electrolyte in the operation voltage window; 3) active in energy storage; and 4) electrically conductive. With such criteria, few materials can be selected as a candidate of volume buffer though some materials have been reported to have negative volume effect such as $LiCoO_2$, [50] A_xVO_2 (A=Li and Na), [9, 13, 41] Li_2MoO_3 [42, 43] and Li_xNbO_2. [23] The negative volume effects of these materials are much less significant than that of the present $Na_{0.5}NbO_2$ (-4.74% for $Na_{0.5}NbO_2 \rightarrow NaNbO_2$ *vs.* -3.17% for $Li_{0.5}CoO_2 \rightarrow LiCoO_2$, -2.72% for $Na_{0.5}VO_2 \rightarrow NaVO_2$, -0.15% for $Li_{0.5}VO_2 \rightarrow LiVO_2$, -0.87% for $Li_{0.5}NbO_2 \rightarrow LiNbO_2$, and -3.66% for $Li_2MoO_3 \rightarrow Li_{0.53}MoO_3$). In short, $Na_{0.5}NbO_2$ meets all these requirements with its obvious negative volume effect and stable structure.

As an active material for Na-ion batteries, $Na_{0.5}NbO_2$ shows excellent electrochemical performances, including high cycling stability (Figure 4b) and prominent rate performance (Figure

4c). After 1500 cycles at 170 mA g^{-1}, the capacity maintains 68.3 mAh g^{-1}, corresponding to a decay of only 0.0047% per cycle. The similarity of the potential profiles (Figure S7) and Raman spectra (Figure S7) of samples before and after long-term cycling demonstrates its high cycling and structural stability. Reversible (charge) capacities of 90, 75, 72 and 70 mAh g^{-1} are obtained at current densities of 30, 50, 100 and 170 mA g^{-1}. Even when the current density is increased from 39 to 620 mA g^{-1}, a reversible storage capacity of 45 mAh g^{-1} can still be obtained, referring to 64% capacity retention (Figure 4c). This outstanding rate performance is mainly attributed to its native high conductivity.

The above structural features and electrochemical evaluation suggest that $Na_{0.5}NbO_2$ can be a competent and effective volume buffer. Figure 4d confirms the feasibility of using $Na_{0.5}NbO_2$ as a volume buffer in constructing a composite electrode with micro-MoS_2 (1:1 wt%; the volume expansion of MoS_2 is over 27% when it is converted to Na_2S, $MoS_2 + 4Na^+ + 4e^- \rightarrow Na_2S + Mo$). [47] MoS_2 is chosen because it has a similar structure to $Na_{0.5}NbO_2$ and their structural changes are all along the *c* axis during cycling. Figure 4d shows that the composite shows a reversible capacity of 260 mAh g^{-1}, referring to a capacity contribution of about 450 and 70 mAh g^{-1} for MoS_2 and $Na_{0.5}NbO_2$, respectively. After 50 cycles, the capacity of the composite maintains at 230 mAh g^{-1} while that of pure MoS_2 falls quickly after 20 cycles due to the repeated and severe volume variation. Apparently, addition of $Na_{0.5}NbO_2$ enhances the cycling stability of positive-strain materials. Further, electrochemical impedance spectroscopy (EIS) (Figure S8c) shows that addition of $Na_{0.5}NbO_2$ helps to facilitate the transportation of charge carriers in the cell, resulting in lower impedance. These benefits can be further applied to other materials such as $Na_2Ti_3O_7$ and TiO_2 (Figure S8).

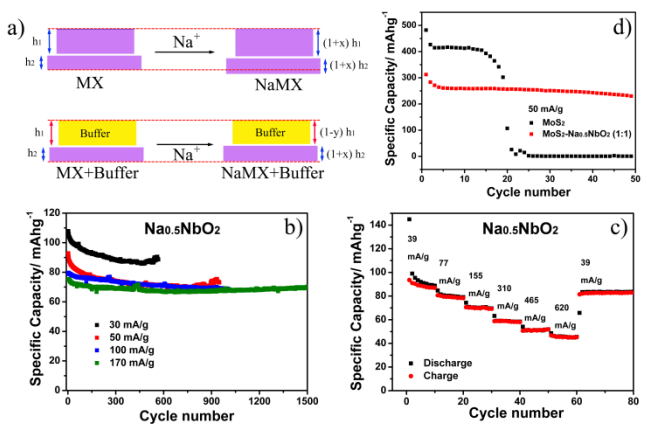

Figure 4. Schematic illustration of volume buffer (a), cycling (b) and rate (c) performances of $Na_{0.5}NbO_2$, cycling performance of MoS_2-$Na_{0.5}NbO_2$ (1:1 wt%) (d). The stable structure and excellent electrochemical performance make $Na_{0.5}NbO_2$ a competent and effective volume buffer for positive-strain electrode materials. As an example of the application of this *buffer* concept, simple composites of negative-strain $Na_{0.5}NbO_2$ and positive-strain MoS_2 show better cycling stability than the MoS_2 alone.

Conclusions

Layer-structured anti-P2 $Na_{0.5}NbO_2$ composed of unusual NbO_6 trigonal prisms and NaO_6 octahedrons is prepared by solid state reactions. Its significant negative volume effect and high structural stability upon Na ion insertion are physically characterized, electrochemically evaluated, and understood by DFT calculations. The weakened Nb-Nb and Nb-O bonding in the O-Nb-O slabs due to the reduction of the Nb ions and the enhanced interlayer interaction are responsible for its negative volume effect. In addition, as an active material for Na-ion batteries, $Na_{0.5}NbO_2$ exhibits prominent cycling stability and rate performance. These distinctive features make it an ideal "volume buffer" to reinforce the cycling stability by compensation for the volume changes of the other phase (component) in a composite electrode. From the aspect of material science and application, our findings emphasize another layered structure with MO_6 trigonal prisms and enrich the understanding of anti-P2 type $Na_{0.5}NbO_2$. From the aspect of energy storage, we present a new type of promising active material for Na-ion batteries and develop an effective "volume buffer" for achieving high energy density batteries with long cycle life.

Actually, the significance of our findings on $Na_{0.5}NbO_2$ is not limited to the above. The variance of the magnetic susceptibility in the 2-20 K temperature range indicates that $Na_{0.5}NbO_2$ is a superconductor and the transition temperature is about 4.5 K (Figure S9). Definitely, these properties are closely correlated with its unique structure and will attract broad interest of, for example, the physicists.

Acknowledgements

This work was financially supported by the National 973 Program of China (Grant Nos.2015CB251100 and 2012CB932302) and the National Natural Science Foundation of China (NSFC Nos. 51372268 and 11234013)

Notes and references

[a] Key Laboratory for Renewable Energy, Chinese Academy of Sciences, Beijing Key Laboratory for New Energy Materials and Devices, Beijing National Laboratory for Condensed Matter Physics, Institute of Physics, Chinese Academy of Sciences, P. O. Box 603, Beijing 100190, China
[b] Laboratory for Advanced Materials & Electron Microscopy, Beijing National Laboratory for Condensed Matter Physics, Institute of Physics, Chinese Academy of Sciences, P. O. Box 603, Beijing 100190, China
[c] X-ray Science Division, Argonne National Laboratory, 9700 South Cass Ave. Argonne, IL 60439 USA
Email: zxwang@iphy.ac.cn;

Author Contributions

The manuscript was written through contributions of all authors. / All authors have given approval to the final version of the manuscript. / ‡These authors contributed equally.

Funding Sources

The authors declare no competing financial interests.

Electronic Supplementary Information (ESI) available: Experimental section; computational section; refined atomic position (Table S1); typical structures (Figure S1); the fitting XRD patterns of anti-P2 and P2 phases (Figure S2); changes of the lattice parameter *c* value (Figure S3); In situ XRD patterns of Na de-intercalation and reintercalation (Figure S4); amount of charge inside the Nb sphere (Figure S5); DOS of NaNbO2 (Figure S6); potential profiles and Raman spectra (Figure S7); cycling performance of $Na_{0.5}NbO_2$ and $Na_2Ti_3O_7$ and TiO_2 (Figure S8); magnetic susceptibility of $Na_{0.5}NbO_2$ (Figure S9). See DOI: 10.1039/b000000x/

1. J. B. Goodenough and Y. Kim, *Chem. Mater.*, 2009, **22**, 587-603.
2. J. M. Tarascon, *Philosophical Transactions of the Royal Society A: Mathematical, Physical and Engineering Sciences*, 2010, **368**, 3227-3241.
3. V. Etacheri, R. Marom, R. Elazari, G. Salitra and D. Aurbach, *Energy Environ. Sci.*, 2011, **4**, 3243-3262.
4. V. Palomares, P. Serras, I. Villaluenga, K. B. Hueso, J. Carretero-Gonzalez and T. Rojo, *Energy Environ. Sci.*, 2012, **5**, 5884-5901.
5. M. H. Han, E. Gonzalo, G. Singh and T. Rojo, *Energy Environ. Sci.*, 2015, **8**, 81-102.
6. N. Yabuuchi, K. Kubota, M. Dahbi and S. Komaba, *Chem. Rev.*, 2014, **114**, 11636-11682.
7. R. Berthelot, D. Carlier and C. Delmas, *Nat. Mater.*, 2011, **10**, 74-80.
8. N. Yabuuchi, R. Hara, M. Kajiyama, K. Kubota, T. Ishigaki, A. Hoshikawa and S. Komaba, *Adv. Energy Mater.*, 2014, **4**, 1301453-1301475.
9. M. Guignard, C. Didier, J. Darriet, P. Bordet, E. Elkaïm and C. Delmas, *Nat. Mater.*, 2013, **12**, 74-80.
10. E. Lee, J. Lu, Y. Ren, X. Luo, X. Zhang, J. Wen, D. Miller, A. DeWahl, S. Hackney, B. Key, D. Kim, M. D. Slater and C. S. Johnson, *Adv. Energy Mater.*, 2014, **4**, 1400458-1400465.
11. A. M. Abakumov, A. A. Tsirlin, I. Bakaimi, G. Van Tendeloo and A. Lappas, *Chem. Mater.*, 2014, **26**, 3306-3315.
12. J. Billaud, R. J. Clément, A. R. Armstrong, J. Canales-Vázquez, P. Rozier, C. P. Grey and P. G. Bruce, *J. Am. Chem. Soc.*, 2014, **136**, 17243-17248.
13. M. Guignard, D. Carlier, C. Didier, M. R. Suchomel, E. Elkaïm, P. Bordet, R. Decourt, J. Darriet and C. Delmas, *Chem. Mater.*, 2014, **26**, 1538-1548.
14. D. Wu, X. Li, B. Xu, N. Twu, L. Liu and G. Ceder, *Energy Environ. Sci.*, 2015, **8**, 195-202.
15. N. Yabuuchi, M. Kajiyama, J. Iwatate, H. Nishikawa, S. Hitomi, R. Okuyama, R. Usui, Y. Yamada and S. Komaba, *Nat. Mater.*, 2012, **11**, 512-517.
16. C. Delmas, C. Fouassier and P. Hagenmuller, *Physica B+C*, 1980, **99**, 81-85.
17. G. Meyer and R. Hoppe, *Z. Anorg. Allg. Chem.*, 1976, **424**, 128-132.
18. D. L. Novikov, V. A. Gubanov, V. G. Zubkov and A. J. Freeman, *Phys. Rev. B*, 1994, **49**, 15830-15835.
19. M. J. Geselbracht, A. M. Stacy, A. R. Garcia, B. G. Silbernagel and G. H. Kwei, *J. Phys. Chem.*, 1993, **97**, 7102-7107.
20. G. Meyer and R. Hoppe, *Angew. Chem., Int. Ed. Engl.*, 1974, **13**, 744-745.
21. K. Takada, H. Sakurai, E. Takayama-Muromachi, F. Izumi, R. A. Dilanian and T. Sasaki, *Nature*, 2003, **422**, 53-55.
22. V. M. Cherkashenko, M. A. Korotin, V. I. Anisimov, V. V. Shumilov, V. R. Galakhov, D. G. Kellerman, V. G. Zubkov and E. Z. Kurmaev, *Z. Phys. B: Condens. Matter*, 1994, **93**, 417-424.
23. N. Kumada, S. Muramatu, F. Muto, N. Kinomura, S. Kikkawa and M. Koizumi, *J. Solid State Chem.*, 1988, **73**, 33-39.
24. N. Kumada, S. Watauchi, I. Tanaka and N. Kinomura, *Mater. Res. Bull.*, 2000, **35**, 1743-1746.
25. M. J. Geselbracht, T. J. Richardson and A. M. Stacy, *Nature*, 1990, **345**, 324-326.
26. E. Moshopoulou, P. Bordet and J. Capponi, *Phys. Rev. B*, 1999, **59**, 9590.
27. M. A. Rzeznik, M. J. Geselbracht, M. S. Thompson and A. M. Stacy, *Angew. Chem., Int. Ed. Engl.*, 1993, **32**, 254-255.
28. D. Larcher and J. M. Tarascon, *Nat. Chem.*, 2015, **7**, 19-29.
29. P. G. Bruce, S. A. Freunberger, L. J. Hardwick and J. M. Tarascon, *Nat. Mater.*, 2012, **11**, 19-29.
30. B. L. Ellis, K. T. Lee and L. F. Nazar, *Chem. Mater.*, 2010, **22**, 691-714.
31. H. Pan, Y.-S. Hu and L. Chen, *Energy Environ. Sci.*, 2013, **6**, 2338-2360.
32. T. Ohzuku, A. Ueda and M. Nagayama, *J. Electrochem. Soc.*, 1993, **140**, 1862-1870.
33. X. Li, X. Ma, D. Su, L. Liu, R. Chisnell, S. P. Ong, H. Chen, A. Toumar, J.-C. Idrobo, Y. Lei, J. Bai, F. Wang, J. W. Lynn, Y. S. Lee and G. Ceder, *Nat. Mater.*, 2014, **13**, 586-592.
34. M. Pasta, C. D. Wessells, N. Liu, J. Nelson, M. T. McDowell, R. A. Huggins, M. F. Toney and Y. Cui, *Nat. Commun.*, 2014, **5**.
35. C. Masquelier, C. Wurm, J. Rodriguez-Carvajal, J. Gaubicher and L. Nazar, *Chem. Mater.*, 2000, **12**, 525-532.
36. A. K. Padhi, K. S. Nanjundaswamy and J. B. Goodenough, *J. Electrochem. Soc.*, 1997, **144**, 1188-1194.
37. Z. Jian, C. Yuan, W. Han, X. Lu, L. Gu, X. Xi, Y.-S. Hu, H. Li, W. Chen, D. Chen, Y. Ikuhara and L. Chen, *Adv. Funct. Mater.*, 2014, **24**, 4265-4272.
38. E. Ferg, R. J. Gummow, A. de Kock and M. M. Thackeray, *J. Electrochem. Soc.*, 1994, **141**, L147-L150.
39. T. Ohzuku, A. Ueda and N. Yamamoto, *J. Electrochem. Soc.*, 1995, **142**, 1431-1435.
40. Y. Wang, X. Yu, S. Xu, J. Bai, R. Xiao, Y.-S. Hu, H. Li, X.-Q. Yang, L. Chen and X. Huang, *Nat. Commun.*, 2013, **4**, 2365-2372.
41. D. Hamani, M. Ati, J.-M. Tarascon and P. Rozier, *Electrochem. Commun.*, 2011, **13**, 938-941.
42. Y.-N. Zhou, J. Ma, E. Hu, X. Yu, L. Gu, K.-W. Nam, L. Chen, Z. Wang and X.-Q. Yang, *Nat. Commun.*, 2014, **5**, 5381-5389.
43. J. Ma, Y.-N. Zhou, Y. Gao, X. Yu, Q. Kong, L. Gu, Z. Wang, X.-Q. Yang and L. Chen, *Chem. Mater.*, 2014, **26**, 3256-3262.
44. H.-F. Roth, G. Meyer, Z. Hu and G. Kaindl, *Z. Anorg. Allg. Chem.*, 1993, **619**, 1369-1373.
45. P. Senguttuvan, G. Rousse, V. Seznec, J.-M. Tarascon and M. R. Palacín, *Chem. Mater.*, 2011, **23**, 4109-4111.
46. H. Pan, X. Lu, X. Yu, Y.-S. Hu, H. Li, X.-Q. Yang and L. Chen, *Adv. Energy Mater.*, 2013, **3**, 1186-1194.
47. X. Wang, X. Shen, Z. Wang, R. Yu and L. Chen, *ACS Nano*, 2014, **8**, 11394-11400.

48. K. Kubota, I. Ikeuchi, T. Nakayama, C. Takei, N. Yabuuchi, H. Shiiba, M. Nakayama and S. Komaba, *J. Phys. Chem. C*, 2015, **119**, 166-175.
49. J. K. Burdett and T. Hughbanks, *Inorg. Chem.*, 1985, **24**, 1741-1750.
50. T. Ohzuku and A. Ueda, *J. Electrochem. Soc.*, 1994, **141**, 2972-2977.